of an active Q-switch device with a 5-nsec pulse width synchronized with the rf structure, this method should be applicable to the beam at LAMPF for producing solitary pulses. In this case, since the solitary pulses have a natural width of 0.25 nsec, the method is expected to be useful in connection with a high-resolution time-of-flight system. Lasers (using Nd–yttrium-aluminum-garnet amplifiers) having the desired characteristics and firing at a rate of 120 pulses per second are currently feasible.

Many people contributed to the success of this effort, in particular D. Cochran, B. Dieterle, D. Gill, R. Hiebert, J. Hontas, C. Hwang, C. Leavitt, J. Seagrave, and the operating staff of the Los Alamos vertical Van de Graaff accelerator.

†Work performed under the auspices of the U. S. Atomic Energy Commission and supported in part by the National Science Foundation under Grant No. GU-3537 and No. GP-20197.

[1]D. Feldman, Z. Naturforsch. A 25, 621 (1970).

[2]L. M. Branscomb and S. J. Smith, Phys. Rev. 98, 1028 (1955).

[3]S. J. Smith and D. S. Burch, Phys. Rev. 116, 1125 (1959).

[4]H. Pilkuhn, *The Interaction of Hadrons* (North-Holland, Amsterdam, 1967), p. 28; and an enlightening discussion with J. D. Finley, III.

Differences in Inner-Shell Vacancy Production for Ar-C Collisions in Gas Versus Solid Targets*

R. C. Der, R. J. Fortner, and T. M. Kavanagh
Lawrence Livermore Laboratory, Livermore, California 94550

and

J. D. Garcia
Department of Physics, University of Arizona,† Tucson, Arizona 85717

(Received 4 November 1971)

X-ray spectra are presented for Ar-C collisions in gas and solid (graphite) targets, for collision energies of 80 and 90 keV. In gas targets, with either carbon or argon as the target, inner-shell vacancies are produced essentially only in the argon L shell. For Ar^+ ions incident on graphite, however, there is a high probability of producing vacancies in the K shell of carbon. These observations are plausibly explained within a diabatic molecular-orbitals framework, and lend strong support to such a description.

In this note we discuss some striking differences in the characteristic x rays produced by energetic heavy ions in gaseous as compared to solid targets. We have examined, in this context, the x-ray spectra from low-energy (< 200 keV) Ar-C collisions. For gaseous targets the data indicate that inner-shell vacancies are produced only in the L shell of argon, whereas in argon bombardment of *solid* carbon (graphite) there is a high probability of producing vacancies in the carbon K shell. These differences are qualitatively explained in terms of projectile stripping and the resultant changes in the quasimolecule formed during the collision.

The experimental technique has been described elsewhere.[1,2] A Bragg spectrometer with a lead-stearate film as the diffracting element was used for observing the x rays emitted at 90° to the direction of the incident beam; the detector was a flow-mode proportional counter with an ~2000-Å-thick Parylene window. Gaseous argon and carbon (methane) targets consisted of a gas cell with a small entrance aperture for the beam and a Parylene window for transmitting the x rays; gas pressures were typically maintained at $\sim 5\times10^{-2}$ Torr. To eliminate effects of Ar^+-Ar collisions due to argon buildup in the graphite target, a clean target spot was used for each data point during these runs; small buildup effects in certain regions of the spectra during the few minutes required to obtain a datum point were removed by using a technique described elsewhere.[3] There was no evidence of argon buildup in the methane target.

Figure 1 shows spectral data for the gas targets. Figure 1(a) is for 90-keV Ar^+ ions incident on methane gas, and also shows the carbon K-x-ray spectrum obtained by 90-keV proton bombardment of the same target. Figure 1(b) is for 80-keV C^+ ions on argon gas, and Fig. 1(c) shows

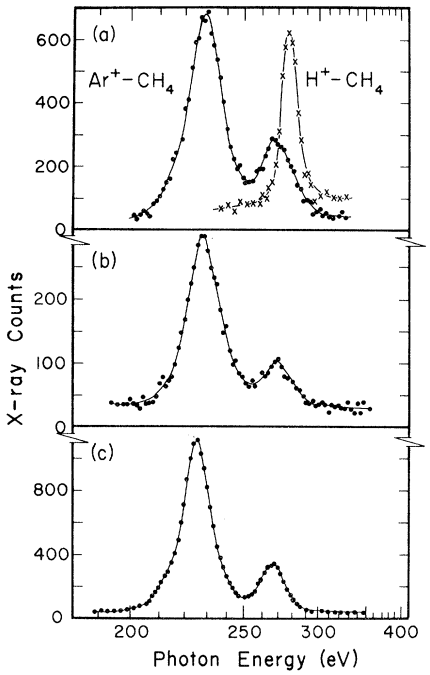

FIG. 1. X-ray spectra for gas targets: (a) 90-keV Ar^+ and protons incident on CH_4; (b) 80-keV C^+ on Ar; (c) 80-keV Ar^+ on Ar.

a spectrum obtained for 80-keV Ar^+-Ar collisions. The spectra for Ar^+-CH_4, C^+-Ar, and Ar^+-Ar are essentially the same, and therefore result from excitation of argon. (The small differences observed in the three spectra can easily be due to differences in collision velocities and the details of outer-shell excitation. Note that the data do not rule out the possibility of a very weak carbon K-x-ray contribution to the spectra for Ar^+-CH_4 and C^+-Ar.)

Figure 2 shows a spectrum for 90-keV Ar^+ bombardment of graphite; while the Ar^+-graphite collision system differs from that represented in Fig. 1(a) *only* in the form of the carbon target, the spectrum is markedly different. There is a strong x-ray component, not evident in the gas-target data, at the position of the carbon K x ray (~277 eV). In addition to the 277-eV line, Fig. 2 also shows a broad low-energy structure which must, because of its energy, be associated with excitation of argon. Note that in Fig. 2 the carbon K-x-ray energy is indicated by a spectrum taken for 90-keV protons incident on the graphite target.

The data in Figs. 1(a) and 1(b) for Ar^+-CH_4 and C^+-Ar, like those in Fig. 1(c) for Ar^+-Ar, are explained in terms of L-shell vacancy production

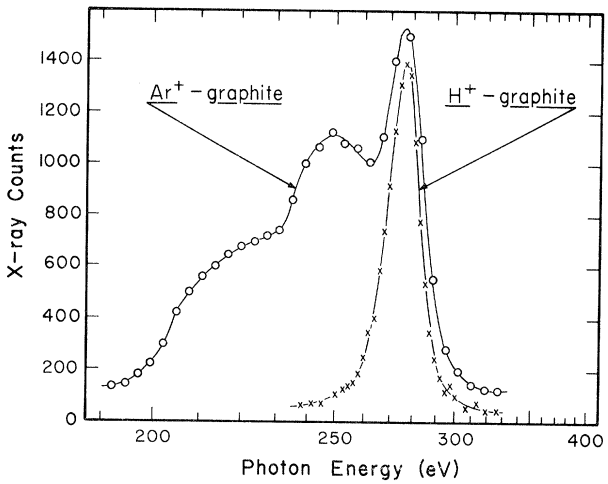

FIG. 2. X-ray spectra for 90-keV Ar^+ and protons incident on a graphite target.

in argon. (See Ref. 1 for a discussion of argon L-vacancy effects for the Ar^+-Ar system.) The low-energy line represents the normal $3s$-$2p$ transition and the peak at ~266 eV is from $3d$-$2p$ transitions. The apparent absence of carbon K x rays in the spectra in Figs. 1(a) and 1(b) is consistent with a diabatic molecular-orbitals description of the collision. In the upper diagram of Fig. 3 we show a schematic correlation diagram[4] for the Ar-C system. (This diagram shows molecular orbitals for the system as a

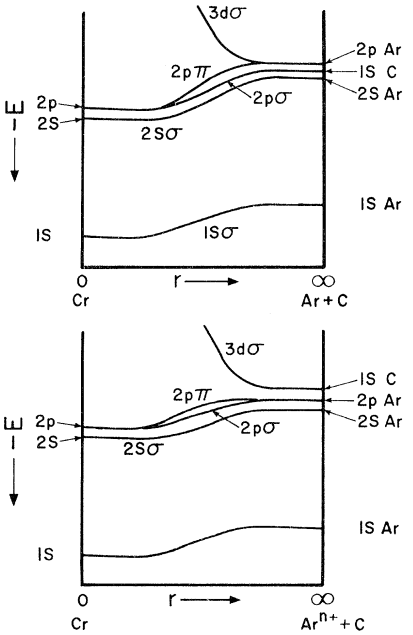

FIG. 3. Diabatic molecular-orbitals diagrams for the Ar-C collision. For simplicity only inner shells are included.

function of collision distance of closest approach; at the right, for large separation, we have the atomic levels of argon and carbon, and at the left, for zero separation, the levels are the atomic levels of the combined atom.) Note that both Ar^+-C and C^+-Ar have the same correlations; and, since we are concerned only with interacting K and L shells, the Ar^+-CH_4 collision should also be discussed using this diagram (i.e., the effects of hydrogen bonded to carbon in the methane molecule are, in this context, not important). We see that the carbon K shell correlates, via a $2p\sigma$ molecular orbital, with the united-atom $2p$ state, and thus carbon K electrons have a very low probability of being "promoted." (Note that all the orbitals shown are full.) The argon $2p$ level, on the other hand, correlates via the steeply rising $3d\sigma$ orbital to the united-atom $3d$ level; the $3d\sigma$ orbital crosses with several higher levels (not shown) and probably couples strongly to the continuum through nonadiabatic terms, thus providing mechanisms for vacancy production. The promotion of electrons during the collision into the normally empty $3d$ level of argon—as required to explain the observed $3d$-$2p$ decays (particularly for C^+-Ar in which the argon cannot experience other collisions prior to inner-shell excitation)—is easily explained in terms of crossings of the $3d\sigma$ orbital with higher levels.

While the Ar^+-CH_4 and C^+-Ar data are in accord with the above molecular-orbitals discussion, the data for Ar^+ bombardment of graphite are not. In particular, there is no mechanism for explaining the prominent peak shown in Fig. 2 and attributed to carbon K-vacancy production. It is expected, however, that an energetic ion traversing a solid is in a highly excited state, and if the initial state of the argon ion at the time of the collision has substantial M-shell excitation, the correlations change. The lower diagram in Fig. 3 shows the correlations for the Ar^{n+}-C system, where n is sufficiently large that the argon $2p$ binding energy exceeds the carbon $1s$ energy ($n \gtrsim 3$). Now it is observed that the carbon $1s$ level correlates to the united-atom $3d$ level, and the carbon should get the vacancies.

It should be noted that the excitation *prior* to the collision is the determining factor for this switchover in the correlation diagrams in Fig. 3, i.e., for determining whether inner-shell vacancies are produced in carbon or in argon. This is to be contrasted with the state of excitation *after* the collision which manifests itself in shifts in the positions of the x-ray lines. The broad low-energy structure in the Ar^+-graphite data (Fig. 2) is interpreted as an unresolved distribution of shifted argon lines, produced in accordance with the *upper* correlation diagram in Fig. 3, but reflecting the distribution of ionization states of the argon ions moving in graphite. (The broad hump at ~250 eV is consistent, for example, with Hartree-Fock calculations[5] for $3s$-$2p$ transitions in argon ions with five or six outer-shell vacancies at the time of x-ray emission. Note that higher final charge states will be accentuated in the x-ray spectra because of their higher fluorescence yields.[6] Double L-shell vacancies in argon can also produce ~250-eV components[1]; such components would, however, also be expected in the gas-target data.) This kind of shift, due to alteration of inner-shell screening, was referred to earlier in connection with slight differences in the argon x-ray spectra in Fig. 1.

Spectra for Ar^+-graphite taken at 45 and 180 keV (in addition to the one at 90 keV shown in Fig. 2) show that the relative probability of producing carbon K x rays—as opposed to argon excitations—increases with increasing bombarding energy. This is consistent with the expected increase in the probability of outer-shell stripping with increased projectile velocity. Note that this kind of measurement provides insight into the distribution of inner-shell binding energies for the argon ion in graphite, *prior to the violent collision*; this, coupled with calculations relating binding energy to defect configurations (e.g., Hartree-Fock, Hartree-Fock-Slater) can provide a method for charge-state determinations for ions moving in solids.

The authors wish to thank Dr. J. M. Khan and Dr. M. E. Cunningham for valuable assistance in early phases of this work.

---

*Work performed under the auspices of the U. S. Atomic Energy Commission.

†Work supported in part by grants from the National Aeronautics and Space Administration, the U. S. Office of Naval Research, and the U. S. Office of Aerospace Research.

[1]M. E. Cunningham, R. C. Der, R. J. Fortner, T. M. Kavanagh, J. M. Khan, C. B. Layne, E. J. Zaharis, and J. D. Garcia, Phys. Rev. Lett. 24, 931 (1970).

[2]R. C. Der, T. A. Boster, M. E. Cunningham, R. J. Fortner, T. M. Kavanagh, and J. M. Khan, Rev. Sci. Instrum. 41, 1797 (1970).

[3]R. C. Der, R. J. Fortner, T. M. Kavanagh, J. M. Khan, L. R. Mervine, and E. J. Zaharis, Rev. Sci. Instrum. 42, 1072 (1971).

[4]The rules for construction of asymmetric molecular-orbital correlation diagrams are given by S. S. Gershtein and V. K. Krivchenkov, Zh. Eksp. Teor. Fiz. 40, 1491 (1961) [Sov. Phys. JETP 13, 1044 (1961)]. We thank M. Barat and W. Lichten for bringing them to our attention.

[5]F. P. Larkins, J. Phys. B: Proc. Phys. Soc., London 4, 1 (1971).

[6]F. P. Larkins, J. Phys. B: Proc. Phys. Soc., London 4, L29 (1971).

Ultrasonic Determination of Anisotropic Shear and Bulk Viscosities in Nematic Liquid Crystals*

K. A. Kemp and S. V. Letcher
University of Rhode Island, Physics Department, Kingston, Rhode Island 02881
(Received 12 October 1971)

Ultrasonic absorption measurements made in the nematic liquid crystals *p*-azoxyanisole and *p*-azoxyphenetole, which were oriented by an external magnetic field, are used to calculate anisotropic viscosity coefficients. Values of α/f^2 and the anisotropy of α/f^2 are found to be frequency independent for frequencies of 5–18 MHz in *p*-azoxyanisole and 3–15 MHz in *p*-azoxyphenetole. The relative angular orientation dependence of the two materials is similar.

Early ultrasonic absorption measurements in liquid crystals were made in unoriented materials and were largely directed toward the critical-point phenomena that occur at the phase transition from liquid crystal to isotropic liquid.[1-3] Recently the anisotropy of the absorption in oriented nematics was demonstrated by measurement of the relative absorption as a function of orientation angle.[4,5] Theoretical developments[6,7] have yielded an expression for sound absorption in oriented nematics in terms of five viscosity coefficients that characterize the dissipative properties of the material. Light-scattering measurements,[8] shear-wave-reflection measurements,[9] and steady-state shear-viscosity measurements[10] have provided values for some coefficients, but, to our knowledge, no anisotropic viscosity coefficients have yet been derived from longitudinal ultrasonic data. From the experimental results presented here, viscosity coefficients for para-azoxyanisole (PAA) and para-azoxyphenetole (PAP) are calculated.

In this study a pulse technique has been used to measure the velocity and absorption of longitudinal ultrasonic waves propagated in bulk liquid-crystal samples at known angles θ with respect to an applied magnetic field (3.5 kOe). The long molecules of these samples line up with their major axes parallel to the applied magnetic field. The sound path length ranged from approximately 0.5 to 5 cm. The orientation dependence of the absorption was measured with the aid of a Matec pulse-amplitude monitor. The temperature of the samples was controlled to within ±0.1°C by a circulating oil bath or by cartridge heaters imbedded in a copper block. The work was performed under an argon cover gas to reduce the possibility of contamination. The samples, obtained from Eastman Organic Chemicals, were recrystallized in acetone at least twice before use.

Absorption data for orientation angles $\theta = 0°$ and 90° (corrected for diffraction loss) are shown in Figs. 1 and 2. Here α is the absorption coefficient and f is the frequency. The anisotropy in α/f^2, i.e., the difference between the 0° and 90° values, changes very slightly with temperature compared to the change in α/f^2 itself. The error ranges shown represent the calculated

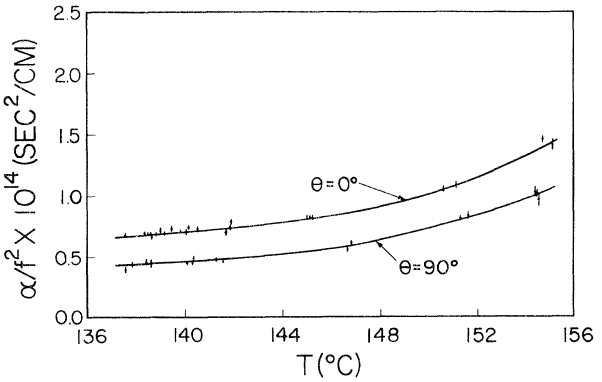

FIG. 1. Temperature dependence of α/f^2 for orientation angles of 0° and 90° (propagation parallel and perpendicular to the magnetic field direction, respectively) for PAA, which is mesomorphic from about 116°C to about 136°C. Data for 5, 10, 14, and 18 MHz are included. Curves are fitted by least squares to the data points with the use of an equation of the form $\alpha/f^2 = A + BT + CT^2 + DT^3$.